Cosmological Constraints from Strong Gravitational Lensing in Clusters of Galaxies

Eric Jullo,[1,2] Priyamvada Natarajan,[3*,4] Jean-Paul Kneib,[2]
Anson D'Aloisio,[4] Marceau Limousin,[2,5] Johan Richard,[6] and Carlo Schimd[2]

[1]Jet Propulsion Laboratory, California Institute of Technology, Pasadena, CA 91109
[2]Laboratoire d'Astrophysique de Marseille, CNRS, Universite de Provence, 38 rue Frederic Joliot-Curie, 13388 Marseille Cedex 13, France
[3]Department of Astronomy, Yale University, P. O. Box 208101, New Haven, CT 06511-8101, USA
[4]Department of Physics, Yale University, P. O. Box 208120, New Haven, CT 06520-8120, USA
[5]Dark Cosmology Centre, Niels Bohr Institute, University of Copenhagen, Juliane Maries Vej 30, 2100 Copenhagen, Denmark
[6]Institute for Computational Cosmology, Department of Physics, Durham University, South Road, Durham, DH1 3LE, UK

*To whom correspondence should be addressed; E-mail:priyamvada.natarajan@yale.edu.

Current efforts in observational cosmology are focused on characterizing the mass-energy content of the Universe. We present results from a geometric test based on strong lensing in galaxy clusters. Exploiting high resolution images from the *Advanced Camera for Surveys* **aboard the** *Hubble Space Telescope* **and extensive ground-based spectroscopic follow-up of the massive galaxy cluster Abell 1689, we used a parametric model to simultaneously constrain the cluster mass distribution and dark energy equation of state. Combining our cosmological constraints with those from X-ray clusters and the** *Wilkinson Microwave Anisotropy Probe* **5-year data gives** $\Omega_{\rm m} = 0.25 \pm 0.05$ **and** $w_{\rm x} = -0.97 \pm$

0.07 **which is extremely competitive with other methods. Inclusion of our method with all other techniques available brings down the current 2σ contours on the dark energy equation of state parameter $w_{\rm x}$ by about 30%.**

Measurements of the Hubble diagram for Type Ia supernovae (*1–4*) combined with constraints from the Wilkinson Microwave Anisotropy Probe (*WMAP5*) (*5, 6*), cosmic shear observations (*7–11*), cluster baryon fractions (*12*), cluster abundances (*13*) and baryon acoustic oscillations (BAO) from galaxy surveys (*14–16*) suggests that $\sim 72\%$ of the total energy density of the Universe is in the form of an unknown constituent with negative pressure - the so-called dark energy. These observations probe the equation-of-state parameter $w_{\rm x}$, defined as the ratio of pressure to energy density, through its effect on the expansion history and structure of the Universe. The current goal of cosmology is to understand the properties of dark energy. In the currently favored flat ΛCDM model[1], dark energy is attributed to a cosmological constant, for which $w_{\rm x} = -1$. Type Ia supernovae, baryon acoustic oscillations, cluster abundances and cosmic shear appear to be very promising techniques to tighten constraints on the equation-of-state parameter in the near future. Because all of these techniques have biases, systematics and degeneracies, it is only in combination that robust estimates of cosmological parameters can be obtained.

The most recent census from a combination of techniques suggests that $\sim 72\%$ of the energy density in the Universe is in the form of dark energy that is powering the accelerating expansion of the Universe. In the progression towards placing tighter constraints on the dark energy equation of state, systematic errors are a major concern. One way forward lies in combining as many independent cosmological tests as possible.

In this work, we present results from a technique that exploits the strong gravitational lens-

[1]The currently favored 'concordance' cosmological model that best describes the Universe is the ΛCDM paradigm in which the bulk of the matter and energy density are dominated by dark matter and dark energy with baryons contributing only $\sim 5\%$.

ing of distant background galaxies by massive galaxy clusters. Through their effect on the local space-time geometry, massive foreground structures cause the deflection and shearing of light rays originating from distant sources. In the case of strong lensing, the light beams are deflected so strongly that they can often result in the observation of several distorted images of a given single background galaxy. The positions of these multiple images depend strongly on the detailed properties of the lens mass distribution (*17–19*). Since the image positions also depend on the angular diameter distance ratios between the lens, source and observer, they encapsulate information about the underlying cosmology. We capitalize on this dependence on the geometry to derive constraints on the cosmological parameters $\Omega_{\rm m}$ and $w_{\rm x}$.

Constraining the energy content of the Universe using multiple sets of arcs in cluster lenses has been explored in the past (*20–26*). In particular, simultaneous inversion of the lens and derivation of cosmological constraints can be performed based on the cosmological sensitivity of the angular size-redshift relation with sources at distinct redshifts (*21*). In this method, the angular diameter distance ratios for 2 images from different sources defines the 'family ratio' Ξ, from the cosmological dependence of which constraints on $\Omega_{\rm m}$ and $w_{\rm x}$ are extracted:

$$\Xi(z_{\rm l}, z_{\rm s1}, z_{\rm s2}; \Omega_{\rm M}, \Omega_{\rm X}, w_{\rm X}) = \frac{D(z_{\rm l}, z_{\rm s1})}{D(0, z_{\rm s1})} \frac{D(0, z_{\rm s2})}{D(z_{\rm l}, z_{\rm s2})} \tag{1}$$

where $z_{\rm l}$ is the lens redshift, $z_{\rm s1}$ and $z_{\rm s2}$ are the two source redshifts, and $D(z_1, z_2)$ is the angular diameter distance.

Application of this method to the cluster Abell 2218 using 4 multiple image systems at distinct redshifts, resulted in $\Omega_{\rm m} < 0.37$ and $w_{\rm x} < -0.80$ for a flat Universe (*25*). A recent feasibility study demonstrates that the degeneracies of this technique are entirely distinct from other cluster methods and that combining the results from several simulated clusters with > 10 multiple image families in each can provide a powerful probe of dark energy (*26*).

We have applied this technique to the massive, lensing cluster Abell 1689 at redshift $z =$

0.184. Based on images from the Advanced Camera for Surveys (*ACS*) aboard the Hubble Space Telescope (*HST*) this cluster has 114 multiple images from 34 unique background galaxies, 24 of which have secure spectroscopic redshifts (ranging from $z \sim 1$ to $z \sim 5$) obtained with the *Very Large Telescope (VLT)* and *Keck Telescope* spectrographs (*27, 28*). Abell 1689 is amongst the richest clusters in terms of the number density of galaxies in its core. It is also amongst the most luminous of galaxy clusters in X-ray wavelengths, with an absolute X-ray luminosity of $L_X = 20.74 \times 10^{37}$ W (*29*). Observationally, Abell 1689 consists of two groups of galaxies : a dominant one located at the center coincident with the peak of X-ray emission, and a secondary concentration about 1 arcminute North-East of the main one. Studies have shown that this second northern group is at a slightly higher redshift, suggesting thus that these two groups might actually be merging (*30*). The projected mass enhancement produced by such a merging configuration, could therefore explain the stunningly large number of multiple images identified in this cluster. Previous work shows that the mass distribution of Abell 1689 is well modeled with a set of parameterized elliptical pseudo-isothermal lensing potentials (*28*). We utilized the most recent parametric model of Abell 1689, which is able to reproduce the observed image configurations to within an average positional accuracy of 2.87 arcseconds, assuming a ΛCDM cosmology[2] (*28*). Our simplified model that has a total of 21 free parameters consists of two large-scale potentials, a galaxy-scale potential for the central brightest cluster galaxy (BCG), and includes the modeling of 58 of the brightest cluster galaxies. Therefore, we explicitly include the effect of substructure in the lens plane and assigned potentials associated with bright cluster galaxies. The velocity dispersion and scale radii of all but one (the BCG) of the cluster galaxies were assumed to follow empirically motivated scaling relations, which have been previously utilized to model cluster lenses (*31, 32*).

Despite the large number of multiple images observed, not all of them can be utilized to

[2]We solved the lens equation in the source plane for Abell 1689 as it is computationally efficient. Inverting in the lens (image) plane provides additional information but is computationally prohibitive at present.

constrain cosmology. From the initial 114 images, we only used those (i) with robust, measured spectroscopic redshifts; and (ii) excluded those in the regions of the cluster with low S/N in the mass reconstruction. This selection results in the culling of multiple images that lie in the most uncertain regions of the mass distribution. Moreover, we identified several bright spots in some well resolved multiple images, which we used to increase the number of families. Applying criterion (i), resulted in a catalog of 102 images. Imposing criteria (i) and (ii), we obtained a catalog of 28 images arising from 12 families all with measured spectroscopic redshifts Fig. 1. After this selection, the images now provide a total of 32 constraints. We assume flatness as a prior ($\Omega_{\rm tot} = 1$) and fix the Hubble parameter at $H_0 = 74\,{\rm km/s/Mpc}$ (*33*)[3].

For each of the observed image systems with n images, we determine the goodness of fit for a particular set of model parameters using a source plane χ^2,

$$\chi^2 = \sum_{i=1}^{n} \frac{\left[M\left(\vec{\beta}_i - \left\langle\vec{\beta}\right\rangle\right)\right]^2}{\sigma_i^2}, \tag{2}$$

where $\vec{\beta}_i$ is the source plane position corresponding to image i, $\left\langle\vec{\beta}\right\rangle$ is the family barycenter, M is the magnification tensor, and σ_i is the total (observational and modeling) error. The total χ^2 was obtained by summing over families and was used in conjunction with a Markov Chain Monte Carlo (MCMC) sampler to probe the posterior probability density function (PDF) as a function of all relevant model parameters (*34*) (SOM). The key degeneracies with cosmological parameters for this technique arise from the velocity dispersions, ellipticity and core radii of the large scale mass clumps in the model (Fig. 4 in the SOM).

The angular resolution of *HST* images is on the order of 0.1 arcseconds. However, the modeling errors are generally larger due to the complexity of the cluster mass distribution, as well as the effect of intervening structures along the line of sight. We quantified the errors due to the presence of structure along the line of sight using the Millennium Simulation halo

[3]We note that our cosmography test is not sensitive to the value of the Hubble parameter.

catalogs (*35*). We quantified the errors on an image by image basis. By randomly slicing through snapshots of the simulation and tiling them at redshift planes between the observer and the source, we constructed 1000 line-of-sight realizations. We then ray traced through each realization with the Abell 1689 model included to estimate the effect of intervening halos on image positions. In most cases, these line-of-sight halos perturbed image positions but did not alter the multiplicity of the images. These perturbations induce positional displacements of the order of 1 arcsecond. Therefore, about 1 arcsecond of the error between observed image positions and model image predictions can be attributed to the presence of structure along the line of sight behind the cluster. The presence of projected correlated and associated large-scale structure (filaments) increases the cross-section to strong gravitational lensing making these clusters more efficient lenses, however, simulations show that this is a sub-dominant effect to that of unassociated distant large-scale structure. Therefore, the presence of aligned correlated large scale structure at the redshift of the cluster does not scupper the recovery of cosmological parameters [4]

From our extensive earlier work on reconstructing the mass distribution of several massive lensing clusters, we find that the association of dark matter substructures with the locations of the brightest cluster galaxies is well matched by that derived from the Millenium Simulation (*32, 36*). Therefore, the use of luminosity-mass scaling relations to map substructure in the cluster is well supported.

The second potential source of error arises from modeling uncertainties for the substructure in the lens plane. This is likely due to scatter in the assumed scaling relations for the velocity dispersions and scale radii of cluster galaxies. Although the mean correlations between these variables may be well described by simple scaling relations, individual galaxies can deviate

[4]We note that filaments aligned at finite inclinations behind the cluster (thus breaking azimuthal symmetry) do yield larger deviations between the projected and multi-plane models compared to the symmetric case. For the non-symmetric case, the deviations are typically on the same level as the errors due to scatter in the cluster galaxy properties. These deviations are still subdominant to the effects of uncorrelated LOS halos.

substantially from them, introducing errors into the parameter recovery. In order to quantify these modeling errors, we performed Monte Carlo simulations of the lens system assuming a 20% scatter in the galaxy scaling relations. This scatter induced modeling errors on the background galaxy image positions that in some cases were as large as ~ 1 arcsecond. Therefore, the estimated errors from substructure effects in the lens plane and along the line of sight are comparable for the selected multiple image families in Abell 1689.

To start, we use the catalog of 102 images (including images with photometric redshift estimates) and our estimates of the observational and modeling errors to obtain the marginalised PDF in the $\Omega_{\rm m} - w_{\rm x}$ plane. Adding in quadrature the systematic errors identified above to the positional uncertainties, we find a best model for Abell 1689 with a well defined though broad degeneracy between $\Omega_{\rm m}$ and $w_{\rm x}$. The "concordance" model of $\Omega_{\rm m} \sim 0.3$ and $w_{\rm x} \sim -1$ lies within the 1σ contour, but the way the degeneracy is pushed against the prior limits suggests either a bias in the mass modeling, or misidentified images (Fig. 5 in SOM). Simulations show that the errors in photometric redshift determination methods at present are too large and limit the efficiency of our technique and introduce biases. Therefore, we excluded all images with photometric redshifts in our modeling, bringing down the number of image families used from 34 to 24. Even with this cut, some images were badly reproduced with very high RMS positional deviations, in particular, those that lie in complex crowded regions of the cluster (regions where the signal-to-noise of the mass map is low due to the presence of several bright cluster galaxies in close proximity). These outlier images from 16 families highlight complex regions in the lens mass distribution, not handled adequately by our simple parametric model. We typically find that these outlier image systems tend to have higher redshifts; thus they are likely to be more affected by uncertainties in modeling the intervening line of sight structure as well. We thus deliberately disregarded images that lie in the most complex regions in the mass distribution. While the recovery of cosmological parameters is insensitive to the choice of profile,

both the PIEMD and NFW (Navarro-Frenk-White) provide comparable constraints on $w_{\rm x}$ and $\Omega_{\rm m}$, observationally some clusters are better fit to one or the other model. Abell 1689 is best fit with a PIEMD profile. The final culled image catalog thus contains 28 images, derived from 12 families at redshifts ranging from $z_S = 1.15$ to $z_S = 4.86$, all of which are spectroscopically measured (Table S1 and Fig. 1).

Optimising our model with all the spectroscopically selected images, including outlier images does not result in significant constraints on either $\Omega_{\rm m}$ and $w_{\rm x}$ and yields an averaged reduced $\chi^2 = 0.08$. This indicates that the line of sight and scaling relation errors are likely overestimated. Thus, we optimized again but this time excluding the outlier images. In this iteration, we obtained an averaged reduced $\chi^2 \sim 28$, indicating that now the errors were somewhat underestimated (Fig. 2). Owing to the large estimates for the modeling errors, constraints obtained in this fashion from a single cluster lens are fairly modest. However, combining our results with those from X-ray clusters and *WMAP5* leads to $\Omega_{\rm m} = 0.25 \pm 0.05$ and $w_{\rm x} = -0.97 \pm 0.07$ (Fig. 2), which is consistent with the values derived from combining *WMAP5* with SN and BAO, $\Omega_{\rm m} = 0.265 \pm 0.16 \pm 0.025$ and $w_{\rm x} = -0.96 \pm 0.06 \pm 0.12$ (*37*).

Our results when combined with the results from *WMAP5* (*38*), the supernovae "Gold sample" (*4*), SNLS project (*39*) and SNEssence, and the BAO peak from *SDSS* (*16*), give $0.23 < \Omega_{\rm m} < 0.33$ and $-1.12 < w_{\rm x} < -0.82$ at the 99% confidence level (Fig. 3). This combination of all current viable probes brings down the overall error in $w_{\rm x}$ by about 30%. Therefore, the combination of cluster methods with *WMAP5* has comparable potency to the combination of other cosmological probes. The future of this geometric technique to constrain cosmology is very promising as significantly tighter constraints can be obtained with data from the upcoming *James Webb Space Telescope*.

References and Notes

1. A. G. Riess, *et al.*, *AJ* **116**, 1009 (1998).

2. S. Perlmutter, *et al.*, *Nature* **391**, 51 (1998).

3. J. L. Tonry, *et al.*, *ApJ* **594**, 1 (2003).

4. A. G. Riess, *et al.*, *ApJ* **607**, 665 (2004).

5. D. N. Spergel, *et al.*, *ApJS* **170**, 377 (2007).

6. G. Hinshaw, *et al.*, *ArXiv e-prints* **803** (2008).

7. D. J. Bacon, A. R. Refregier, R. S. Ellis, *MNRAS* **318**, 625 (2000).

8. N. Kaiser, G. Wilson, G. A. Luppino, *ArXiv:astro-ph/0003338 Astrophysics e-prints* (2000).

9. L. Van Waerbeke, *et al.*, *A&A* **358**, 30 (2000).

10. D. M. Wittman, J. A. Tyson, D. Kirkman, I. Dell'Antonio, G. Bernstein, *Nature* **405**, 143 (2000).

11. E. Semboloni, *et al.*, *A&A* **452**, 51 (2006).

12. S. W. Allen, R. W. Schmidt, H. Ebeling, A. C. Fabian, L. van Speybroeck, *MNRAS* **353**, 457 (2004).

13. A. Vikhlinin, *et al.*, *ApJ* **692**, 1060 (2009).

14. G. Efstathiou, *et al.*, *MNRAS* **330**, L29 (2002).

15. U. Seljak, *et al.*, *Phys. Rev. D* **71**, 103515 (2005).

16. D. J. Eisenstein, *et al.*, *ApJ* **633**, 560 (2005).

17. J.-P. Kneib, R. S. Ellis, I. Smail, W. J. Couch, R. M. Sharples, *ApJ* **471**, 643 (1996).

18. P. Natarajan, J.-P. Kneib, I. Smail, R. S. Ellis, *ApJ* **499**, 600 (1998).

19. G. P. Smith, *et al.*, *MNRAS* **359**, 417 (2005).

20. B. Paczynski, K. Gorski, *ApJ* **248**, L101 (1981).

21. R. Link, M. J. Pierce, *ApJ* **502**, 63 (1998).

22. A. R. Cooray, J. M. Quashnock, M. C. Miller, *ApJ* **511**, 562 (1999).

23. G. Golse, J.-P. Kneib, G. Soucail, *A&A* **387**, 788 (2002).

24. M. Sereno, *A&A* **393**, 757 (2002).

25. G. Soucail, J.-P. Kneib, G. Golse, *A&A* **417**, L33 (2004).

26. J. Gilmore, P. Natarajan, *MNRAS* **396**, 354 (2009).

27. T. Broadhurst, N. Benítez, D. Coe, et al, *ApJ* **621**, 53 (2005).

28. M. Limousin, *et al.*, *ApJ* **668**, 643 (2007).

29. H. Ebeling, *et al.*, *MNRAS* **281**, 799 (1996).

30. O. Czoske, *IAU Colloq. 195: Outskirts of Galaxy Clusters: Intense Life in the Suburbs*, A. Diaferio, ed. (2004), pp. 183–187.

31. P. Natarajan, J.-P. Kneib, *MNRAS* **287**, 833 (1997).

32. P. Natarajan, *et al.*, *ApJ* **693**, 970 (2009).

33. S. H. Suyu, *et al.*, *ApJ* **711**, 201 (2010).

34. E. Jullo, *et al.*, *New Journal of Physics* **9**, 447 (2007).

35. V. Springel, C. S. Frenk, S. D. M. White, *Nature* **440**, 1137 (2006).

36. P. Natarajan, G. De Lucia, V. Springel, *MNRAS* **376**, 180 (2007).

37. R. Kessler, *et al.*, *ApJS* **185**, 32 (2009).

38. E. Komatsu, *et al.*, *ApJS* **180**, 330 (2009).

39. P. Astier, *et al.*, *A&A* **447**, 31 (2006).

EJ and JPK acknowledge fruitful discussions with Dan Coe, Leon Koopmans, Lexi Moustakas and Matt Auger. The authors are thankful for computational resources from IDRIS/CNRS, JPL and J.-C Bourret. EJ acknowledges receipt of an ESO PhD scholarship and a NASA post-doctoral fellowship. PN acknowledges the support of a Radcliffe Fellowship at Radcliffe Institute for Advanced Study at Harvard, where some of this work was completed. JPK, ML and CS acknowledge support from CNRS. ML thanks CNES and the Ville de Marseille. The authors thank Alexey Vikhlinin for providing us the data on cosmological constraints from X-ray clusters to combine with our strong lensing derived constraints.

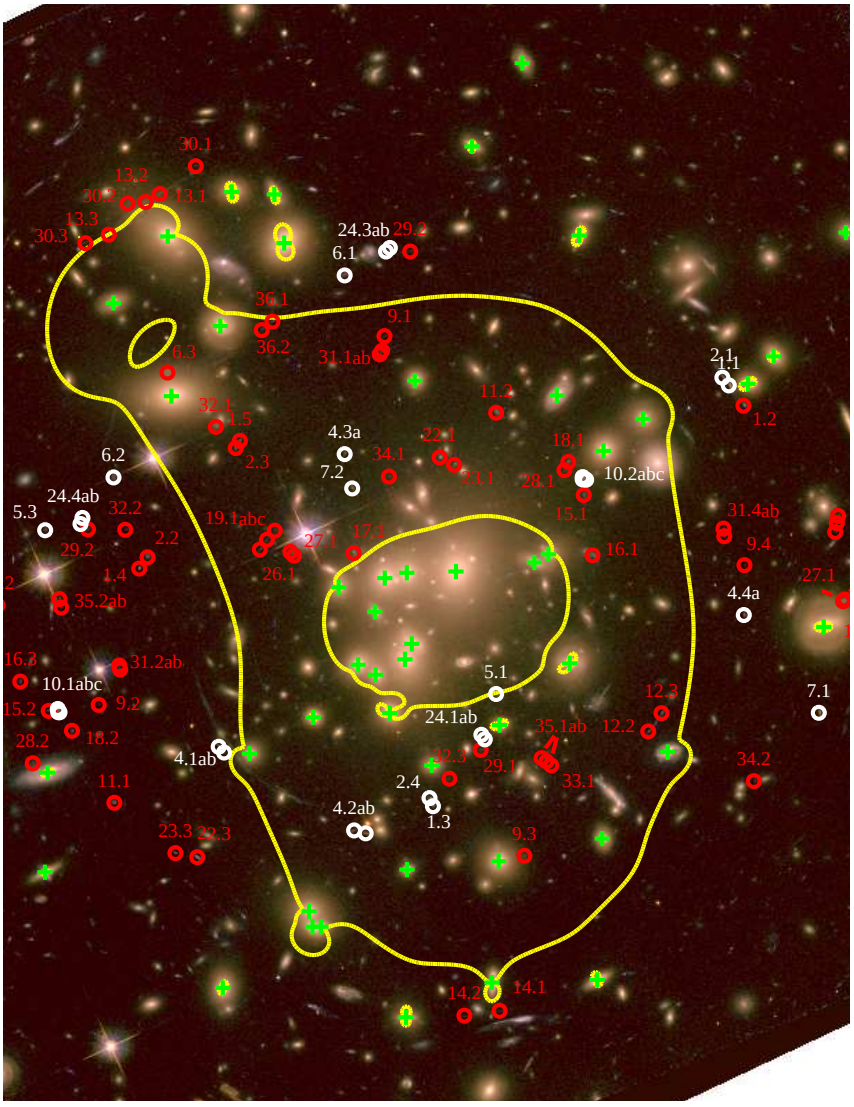

Figure 1: The critical lines for a source at $z = 3$ are overplotted in yellow on the *HST ACS* image of Abell 1689. The lensing mass model used is the one from which we derived cosmological constraints. In addition to 2 large scale clumps and the BCG, this model includes the contribution of 58 cluster galaxies. The positions of cluster galaxies are marked with green crosses. Overplotted in white are the 28 multiple images arising from 12 families that we used in this work; the red circles mark the positions of the rejected images.

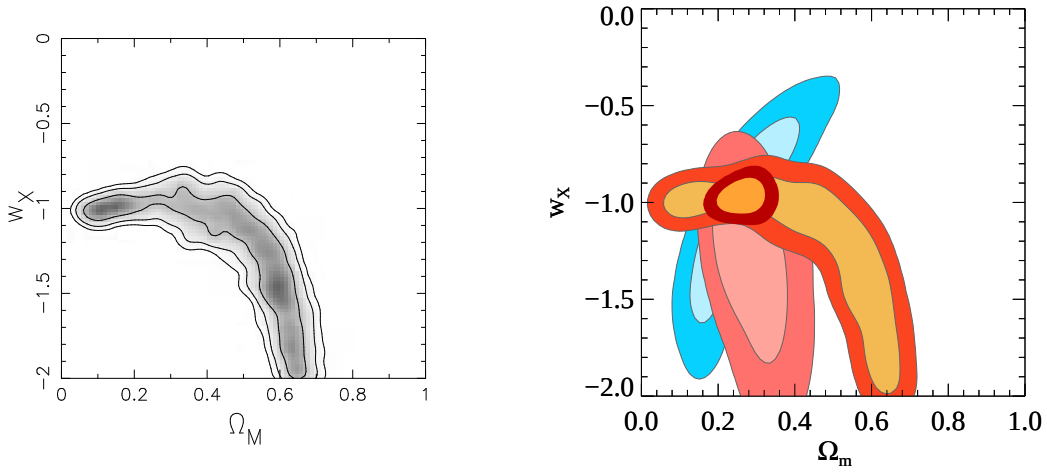

Figure 2: Left) The results from the simultaneous Bayesian optimization of the detailed mass distribution and cosmological parameters in the $\Omega_{\rm m} - w_{\rm x}$ plane for Abell 1689 using the 28 multiple images belonging to 12 families at distinct redshifts as constraints from strong lensing including only observational errors. The plotted contours are the 1, 2 and 3-σ confidence levels. (Right) The results from combining cosmological constraints from *WMAP5*+ evolution of X-ray clusters +cluster strong lensing (cluster only methods); the 1 and 2σ contours are plotted, blue contours - constraints from *WMAP5*, pink contours - X-ray clusters, orange contours - cluster strong lensing. We multiplied the likelihoods for the various techniques to obtain this plot. The degeneracy directions for X-ray clusters and cluster strong lensing are orthogonal.

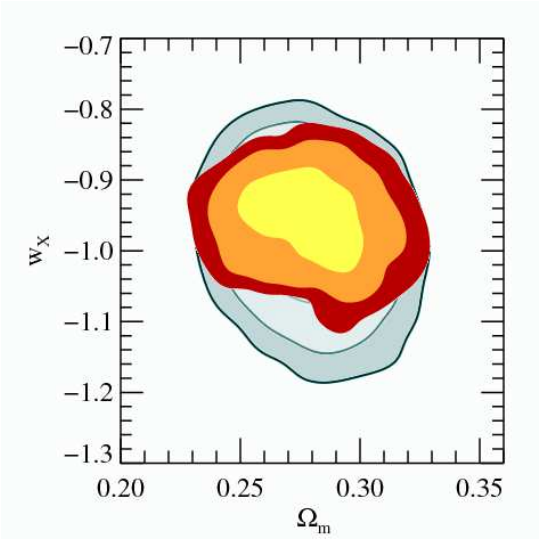

Figure 3: Combination of constraints from strong lensing, the *WMAP5* data (*38*), the supernovae "Gold sample" (*4*), SNLS project (*39*) and SNEssence, and the BAO peak from *SDSS* (*16*). Contours for non-SL cosmological probes come from the *WMAP* plotter. The overplotted contours are all 1, 2 and 3-σ confidence levels.